# Adversarial Media-fusion Approach to Strain Prediction for Bridges

Takaya Kawakatsu[1], Kenro Aihara[2], Atsuhiro Takasu[2] and Jun Adachi[2]
[1]*The University of Tokyo, 2-1-2 Hitotsubashi, Chiyoda, Tokyo, Japan*
[2]*National Institute of Informatics, 2-1-2 Hitotsubashi, Chiyoda, Tokyo, Japan*

Keywords: Generative Adversarial Network (GAN), Civil Engineering, Structural Health Monitoring, Multimodal.

Abstract: This paper contributes to the wide acceptance of autonomous health monitoring for real bridges. Our approach involves dynamic simulation, whereby damage may be identified by detecting abnormal mechanical behavior in the bridge components in response to passing vehicles. Conventionally, dynamic simulation requires expert knowledge of mechanics, components, materials, and structures, in addition to accurate modeling. Moreover, it requires detailed specification of the external forces applied, such as vehicle speeds, loci, and axle weights. This paper introduces a novel media-fusion framework to obtain a bridge dynamic model in a fully data-driven fashion. The proposed generative model also successfully simulated strain responses for a real road bridge by using a camera and strain sensors on the bridge. The generative network was trained by an adversarial learning algorithm customized for media-fusion analysis.

## 1 INTRODUCTION

With the widespread adoption of compact devices and drones, attention is being directed toward a fully automated approach to monitor the health of bridges using sensor fusion involving heterogeneous sensors installed on the target bridge. Our main interest in this paper is the detection of fatal faults that may cause a bridge to collapse, such as fractures and the corrosion of reinforcing rods, girders, and decks. Unfortunately, the mechanisms for damage progression on individual real bridges are yet to be fully clarified. Furthermore, there has been no open collection of ground-truth data for damage identification, which would be helpful for approaches involving data mining.

Studies of damage detection based on mechanics can be classified according to two major approaches. The first uses long-term behavior of the bridge, such as natural vibration (Bicanic and Chen, 1997), which does not depend strongly on individual vehicles. The second uses transient state analysis, which identifies an abnormal movement by the bridge components in response to every passing vehicle (Huang et al., 2016). Compared with the first approach, the second may provide rich information sampled under a variety of traffic conditions. To detect anomalous mechanical responses, the dynamic system of the bridge must be modeled in advance. One powerful solution is to use finite element analysis (FEA) (Wu et al., 2017; Shah et al., 2018). However, FEA requires accurate model making by hand, which is not feasible for the majority of existing bridges.

Our solution is to use a generative neural network that predicts the transient responses for every passing vehicle, which must be observed by sensors installed upon the bridge components. The generative network involves two networks, namely *encoder* and *decoder*. The encoder network collects vehicle properties in a media-fusion fashion that combines a video network and a sensor data network. The video is recorded by a surveillance camera above the bridge entrance and contains rich information about every passing vehicle, including speed, locus (left/right position in the lane), and axle positions. The sensor data are recorded by a strain sensor underneath the bridge deck and contain information about axle weights. The decoder network generates the dynamic response caused by the vehicle, by taking the output of the encoder as its input. That is, our neural network takes the raw sensor-data signal as input and outputs a decoded sensor signal, thereby modeling the transfer function between the sensors.

To realize realistic predictions, we have improved the generative adversarial networks (GANs) (Radford et al., 2016; Goodfellow et al., 2014). In addition, we implemented generative networks which were trained just by minimizing mean squared errors (MSEs). The results in Section 4 demonstrate the effectiveness of our approach to modeling bridge dynamics.



Kawakatsu, T., Aihara, K., Takasu, A. and Adachi, J.
Adversarial Media-fusion Approach to Strain Prediction for Bridges.
DOI: 10.5220/0007555007360743
In *Proceedings of the 8th International Conference on Pattern Recognition Applications and Methods (ICPRAM 2019)*, pages 736-743
ISBN: 978-989-758-351-3

## 2 RELATED WORK

It is usual for a road bridge to bend and distort as a vehicle passes over the bridge. If we assume that all of a vehicle's properties could be obtained in advance, the bridge structural response including normal strain, shear strain and displacement would be predictable by using a bridge model. Existing modeling techniques can be classified according to two major approaches, namely explicit modeling and implicit modeling. The explicit approaches use FEA (Mohamed et al., 2017; Mohamed and Tahar, 2017), where bridge models are typically created manually and optimized by iterative model updates using a test vehicle (Wu et al., 2017). By comparing uninjured and damaged models (Shah et al., 2018), the damage can be localized.

On the other hand, the implicit approach abandons explicit construction of bridge structural models, not least because accurate FEA modeling is costly. In this approach, there are two main methods for anomalous behavior detection. The first method is based on using model parameters that dominate the bridge dynamics, such as natural frequencies (Bicanic and Chen, 1997), damping ratios (Cao et al., 2017), and stress influence lines (Chen et al., 2014). The second method is based on physical observation where the anomaly is defined as a dissociation between sensor data and predictions. The predicted data can be static (Liu and Wang, 2010; Ma and Bi, 2011) or dynamic (Zhang et al., 2018).

Traditionally, the transient signals were explained by using Kalman filtering (Bing et al., 2011; Xiao and Fang, 2016; Quansheng et al., 2010; Palanisamy and Sim, 2015) for the case of quasistatic linear responses. In a recent approach, Neves et al. (Neves et al., 2017; Neves et al., 2018) modeled bridge vibration signals by using a neural network that took previous 5-gram acceleration samples, axle loads, and axle positions as its input.

Aspects of bridge dynamics such as normal strain and displacement can be estimated by introducing the concept of an *influence line* (Chen et al., 2014; Huang et al., 2016). The strain response by components, e.g., flanges, girders, and deck slabs, may be explained by a linear response model where the strain measurement $s(t)$ at time $t$ is proportional to the product of axle load $w(x,t)$ and the value of the influence line $i(x)$ at axle point $x$:

$$s(t) \approx \hat{s}(t) = \int_0^l w(x,t)i(x)dx, \qquad (1)$$

where $l$ is the bridge length. The function $i(x)$ denotes a proportionality factor for $w(x,t)$, which is specific to each bridge.

To predict the dynamic responses or to extract the influence line from sensor data, the vehicle properties, including speed, loci, axle positions, and weights, are needed. Zaurin and Catbas (Zaurin and Catbas, 2011) also investigated the collection of vehicle properties via video surveillance. A problem with their approach was that the targets were limited to test vehicles with known axle loads. The most obvious approach to axle weighing is to use an axle-load meter. However, it is hard to retrofit an axle-load meter to existing bridges because this meter needs paving work for installation. Moreover, an axle-load meter is fragile and requires frequent repair. Additionally, accurate axle weighing may impose severe limits on vehicle traveling speed. An alternative solution uses a bridge weigh-in-motion (BWIM) (Lydon et al., 2015; Yu et al., 2016) system that estimates axle weights by Eq. (1), but if the bridge becomes damaged, the influence line may change and lead to inaccurate axle-load estimates. The influence line may also change its shape if the running position in the lane changes. Accordingly, we must develop a complex model to handle the large number and wide variety of patterns of strain responses collected by test runs in advance.

In a previous paper (Kawakatsu et al., 2018a), we abandoned the collection of axle weights. Instead, we proposed an anomaly-detection method based on the assumption that vehicle appearances and bridge strain responses may share common features for the passing vehicles. As we have previously reported (Kawakatsu et al., 2018b; Kawakatsu et al., 2019), the strain data themselves contain rich information about the passing vehicles. By using two convolutional neural networks (CNNs) for video and strain signals and by comparing the video and sensor data in a common feature space, we could successfully identify anomalous responses. The main problem in this work is the interpretation of anomalous scores that are not directly associated with physical abnormalities.

## 3 MEDIA-FUSION GAN

Fig. 1 illustrates the architecture of the generative network. The network comprises two subnets, namely the encoder and the decoder. The encoder extracts the features of each vehicle, and the decoder predicts the strain signal. Both subnets involve many preactivated residual blocks (He et al., 2016). Note that we applied an additional activation function to the output of each block in addition to the two activation functions inside the block. In this paper, we used leaky ReLU (Maas, 2013) for all activation functions except for those in the output layers.

The encoder network shown in Fig. 1(a) is derived from the *SpiNet* (Kawakatsu et al., 2018a). To obtain

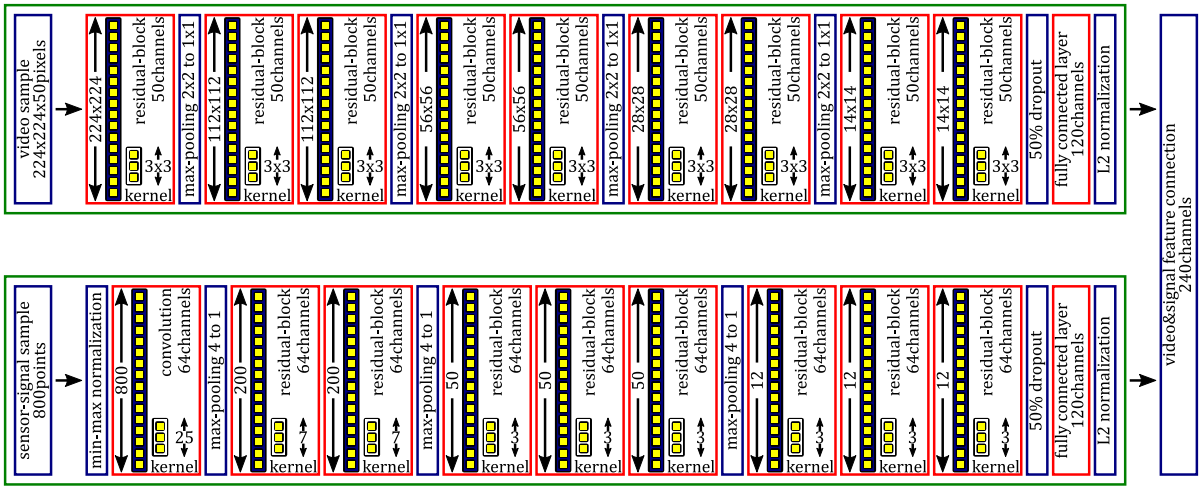


(a) Encoder network.

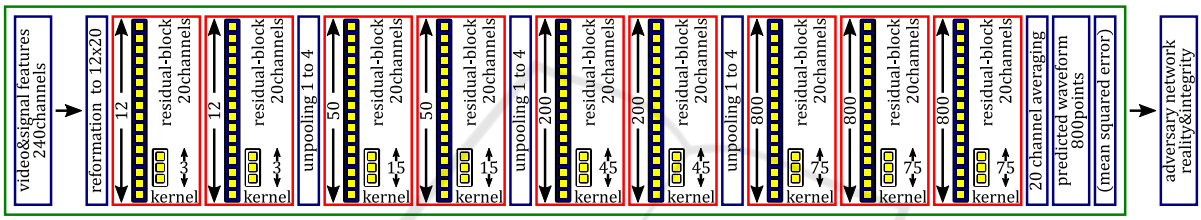


(b) Decoder network.

Figure 1: Media-fusion generator network architecture.

accurate predictions, the parameters of the unknown target vehicle need to be acquired by using sensors on the target bridge. As described in Eq. (1), the required parameters include traveling speed, locus, axle loads, and axle positions. These parameters are obtained by the multimodal encoder, which combines two CNNs for video and strain signals.

First, the video CNN receives 50 grayscale video frames (taken over two seconds) recorded from when the passing vehicle enters the camera's field of view. Each frame is resized to $224 \times 224$ pixels in advance.

Next, the strain CNN receives four-second batches of raw strain signals sampled at 200 Hz. We fed raw signal sequence directly to the CNN, following Dai et al. (Dai et al., 2017). Each sequence starts (or ends) at the same time as the vehicle enters (LtoR) or leaves (RtoL) the bridge. Then, each sample is scaled so that its maximum and minimum values are normalized to 1 and 0, respectively, to enable effective learning.

Finally, the multimodal encoder outputs a feature vector of 240 channels by combining video and signal features of the target vehicle. To suppress overfitting, we inserted a 50% dropout between the last residual block and the following linear layer in each network. In addition, we again normalized the video and signal features individually to enable effective learning.

The decoder network shown in Fig. 1(b) receives the feature vector for each target vehicle and predicts a target waveform of 800 signal points (four seconds), which is rescaled in the same way as the source signal. The decoder was designed as a deep residual network, which upsamples the feature vector by three times to obtain target signals at 200 Hz. The upsampling was performed just by copying each element in the source vector into four neighboring signal points in the target vector. A generous kernel width for each convolution layer was set, similar to WaveGAN (Donahue et al., 2018), to enable the layer to handle the low-frequency signals seen in Fig. 4. The target signal was obtained by averaging 20 channels of the feature vector into a single channel in the final layer.

The generator network was trained introducing the GAN (Goodfellow et al., 2014; Radford et al., 2016) approach. Typically, an adversary network examines whether the generated fake data are as realistic as the observed data (Goodfellow et al., 2014). In addition, our adversary network examines the integrity between the source signal and prediction, which should be high because they were both caused by the same vehicle.

Therefore, our adversary takes a pair comprising two signal sequences from the source sensor signal $\boldsymbol{y}$ and target sensor signal $\boldsymbol{z}$ (or prediction $\hat{\boldsymbol{z}}$), similar to

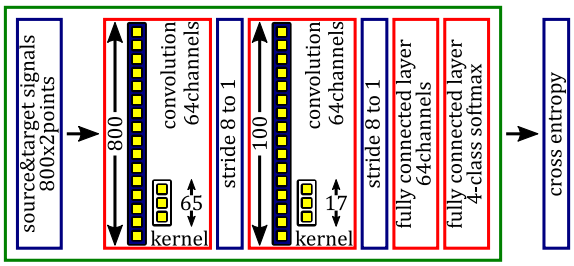


Figure 2: Media-fusion adversary network architecture.

Table 1: Classification problem for the adversary.

| | Real $\boldsymbol{z}$ | Fake $\hat{\boldsymbol{z}}$ |
|---|---|---|
| Consistent | $\{\boldsymbol{y}_n, \boldsymbol{z}_n\}$ | $\{\boldsymbol{y}_n, \hat{\boldsymbol{z}}_n \sim G(\boldsymbol{x}_n, \boldsymbol{y}_n)\}$ |
| Inconsistent | $\{\boldsymbol{y}'_n, \boldsymbol{z}_n\}$ | $\{\boldsymbol{y}'_n, \hat{\boldsymbol{z}}_n \sim G(\boldsymbol{x}_n, \boldsymbol{y}_n)\}$ |

pix2pix (Isola et al., 2017), and classifies the pair into four classes, as shown in Table 1. These four types of pairs are created uniformly for each $n$-th observation sample $\{\boldsymbol{x}_n, \boldsymbol{y}_n, \boldsymbol{z}_n\}$ by the sampling function $s_k$:

$$s_1(n) = \{\boldsymbol{y}_n, \boldsymbol{z}_n\}, \tag{2}$$

$$s_2(n) = \{\boldsymbol{y}'_n, \boldsymbol{z}_n\}, \tag{3}$$

$$s_3(n) = \{\boldsymbol{y}_n, G(\boldsymbol{x}_n, \boldsymbol{y}_n)\}, \tag{4}$$

$$s_4(n) = \{\boldsymbol{y}'_n, G(\boldsymbol{x}_n, \boldsymbol{y}_n)\}. \tag{5}$$

$\boldsymbol{y}'_n$ was selected from the samples other than $\boldsymbol{y}_n$ in the mini batch in each training iteration. Accordingly, $4N$ pairs were fed to the adversary for $N$ samples during the training.

Fig. 2 illustrates the architecture of the adversary network. We modified the Model 1 CNN proposed in a previous paper (Kawakatsu et al., 2019) to take the source sensor signal $\boldsymbol{y}$ and target signal $\boldsymbol{z}$ as the input. The adversary is shallower than the generator, which may suppress overfitting. The target signal input may comprise real or fake strain sequences, while the other input is always real but is sometimes inconsistent with the target signal. The loss function for the adversary $D$ is defined as the cross entropy for the four classes:

$$\mathcal{L}_D = \frac{1}{N}\sum_{n=1}^{N}\frac{1}{4}\sum_{k=1}^{4}\log D(k\|s_k(n)), \tag{6}$$

where $D$ takes a pair created by $s_k$ selected uniformly as input and predicts the probability that the input pair is classified to the $k$-th class in Table 1.

The generator $G$ was trained so that the prediction $\hat{\boldsymbol{z}}$ looks real and consistent with the observation $\boldsymbol{y}$. To stabilize the GAN optimization process, we added an auxiliary MSE element to the cross entropy, following Yang et al. (Yang et al., 2017) to obtain Eq. (7).

$$\mathcal{L}_G = \frac{1}{N}\sum_{n=1}^{N}\left\{\log D(1\|s_3(n)) + \lambda\|\hat{\boldsymbol{z}} - \boldsymbol{z}\|^2\right\}, \tag{7}$$

where $\lambda$ was set to 1. Both networks were trained in a mini-batch fashion that the losses $\mathcal{L}_G$ and $\mathcal{L}_D$ were minimized. In each training iteration, $G$ was updated first and then $D$ was updated.

It should be noted that our generator did not take a random noise variable as input, unlike the previous GAN studies (Goodfellow et al., 2014; Radford et al., 2016), because we required deterministic models and the contribution of the random input was not obvious in our study. In future work, we may explore a method for handling non-deterministic behavior of the bridge by exploiting random variables in future work.

## 4 EXPERIMENTAL RESULTS

Section 4 demonstrates our generative network for the case of a 300-m prestressed concrete (PC) bridge in Japan, denoted Bridge C, which has two lanes and four spans. We deployed a traffic surveillance camera at the bridge entrance to capture images of vehicles in close proximity to the vehicles. We also installed four strain sensors beneath the bridge deck to collect strain signals in the direction orthogonal to the bridge axis. These sensors are shown as four red triangles denoted as S1P4, S2P4, S3P4, and S4P4 in Fig. 3. The strain sensor model was PKM-50S, manufactured by Tokyo Measuring Instruments Laboratory, Co. Ltd. We also installed an accelerometer at the center of the leftmost span, as shown by the yellow triangle denoted A3ZP8 in Fig. 3. All of the sensors were synchronized except for the camera, and their sampling rate was 200 Hz. The frame rate of the camera was then set to 25 frames per second.

Fig. 4 show two examples of the observed signals after a large vehicle entered Bridge C from left to right (LtoR) and from right to left (RtoL). The signal peaks indicate the times when a wheel axle passed over the sensor. As investigated previously (Kawakatsu et al., 2018b; Kawakatsu et al., 2019), the response signals contain various information about the vehicles, which may include speed, loci, and axle numbers, although the accuracy may be lower than that derived from the video. However, axle weights may be better obtained from strain data than from video data.

In preparation for the experiments, we needed to collect times when vehicles entered or left the bridge. For this purpose, we utilized the traffic dataset DS601 prepared previously (Kawakatsu et al., 2019). DS601 was created automatically using Faster R-CNN (Ren et al., 2015) and contains information about 996,093 vehicles which crossed over the bridge between 08:00 and 16:00 from November 2016 to April 2017. In this work, we ignored all vehicles with two axles because

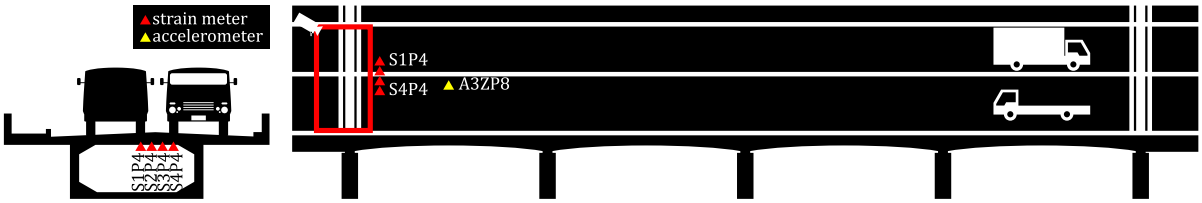


Figure 3: Installation positions of strain sensors and an accelerometer on Bridge C.

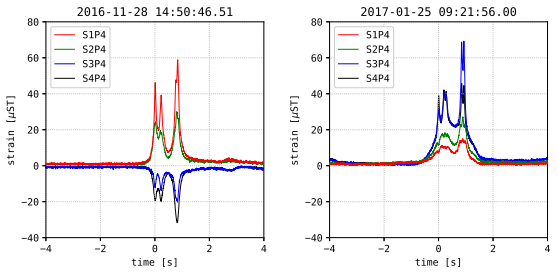


(a) An LtoR vehicle. (b) An RtoL vehicle.

Figure 4: Examples of strain responses caused by vehicles.

civil engineers are mainly interested in large vehicles.

We then collected videos of the target vehicles and strain signals caused by the vehicles. The *n*-th vehicle record is described as a triplet $\{\boldsymbol{x}_n, \boldsymbol{y}_n, \boldsymbol{z}_n\}$ composed of a video $\boldsymbol{x}$, source sensor signal $\boldsymbol{y}$, and target signal $\boldsymbol{z}$ for the *n*-th vehicle. The traffic dataset was divided randomly into two subsets, namely *trainval* data and *evaluation* data. In addition, 20% of the *trainval* data were assigned as *validation* data, while the remaining 80% were assigned as *training* data. The training data were utilized for the generator optimization, while the validation dataset was utilized for early stopping (Yao et al., 2007). The evaluation was performed only once using a model that updated the minimum of the MSE for the validation data. The trainval dataset therefore involved 17,757 LtoR and 20,996 RtoL vehicles, and the evaluation data involved 17,967 LtoR and 21,078 RtoL vehicles.

We implemented two derivative generator models on Chainer[1]5.0.0. One was the GAN model described in Section 3, and the other was a MSE model trained without the GAN mechanism. They were accelerated by a GPU (NVIDIA GeForce GTX 1080 Ti), utilizing CUDA[2]9.2. We also employed the AMSGrad (Reddi et al., 2018) for optimization, and the mini-batch size was set to 10. The two models were trained over 200 epochs, and the evaluation processes were performed in the manner of early stopping (Yao et al., 2007).

First, we evaluated the signal correlation between the observation $\boldsymbol{z}$ and the prediction $\hat{\boldsymbol{z}}$. Unfortunately, there are no accepted metrics for waveform similarity

[1]http://chainer.org

[2]http://developer.nvidia.com/cuda

Table 2: Kendall $\tau$ coefficients and MSEs for the GAN.

| Lane | Source | Target | $\overline{\tau}$ | $\overline{\|\hat{\boldsymbol{z}} - \boldsymbol{z}\|_2^2}$ |
|---|---|---|---|---|
| RtoL | S1P4 | S3P4 | 0.747 | 2.756 |
| | | S4P4 | 0.730 | 3.035 |
| | S2P4 | S3P4 | 0.756 | 2.645 |
| | | S4P4 | 0.720 | 3.015 |
| LtoR | S3P4 | S1P4 | 0.748 | 1.242 |
| | | S2P4 | 0.687 | 2.018 |
| | S4P4 | S1P4 | 0.691 | 1.268 |
| | | S2P4 | 0.674 | 1.881 |

beyond squared distance and cross-correlation. In this work, we focused on the fact that the values of signal points could be estimated by a linear combination of influence lines and therefore evaluated the correlation between the signal points of the ground truth and the prediction. It should be noted that the distributions of the signal values were not uniform but biased strongly toward 0 $\mu$ST, as shown in Fig. 4. Therefore, we used the rank correlation coefficient $\tau$'s (Kendall, 1938) as metrics. Table 2 shows the average $\tau$ coefficients and the MSEs for the evaluation data. From these results, the proposed GAN model was able to achieve a strong correlation between observation and prediction.

After the waveform prediction for the evaluation dataset, we sorted the waveforms in terms of squared error and extracted the first and third quantiles. Fig. 5 shows examples of strain responses for LtoR vehicles passing over strain sensor S1P4, which were predicted using sensor S4P4. The numbers in brackets indicate the anomaly scores (Kawakatsu et al., 2018a) for real and fake signals. For both quantiles, the GAN model generated realistic signals that were indistinguishable from the real observation data. As seen in Fig. 5, the waveforms generated by the MSE model were much smoother than those obtained by the GAN model. The GAN simulated not only the macroscopic signals but also the noise components. The strain peaks indicate the times at which axles passed over the sensors, and the two generators successfully simulated these peaks both in terms of peak heights and times.

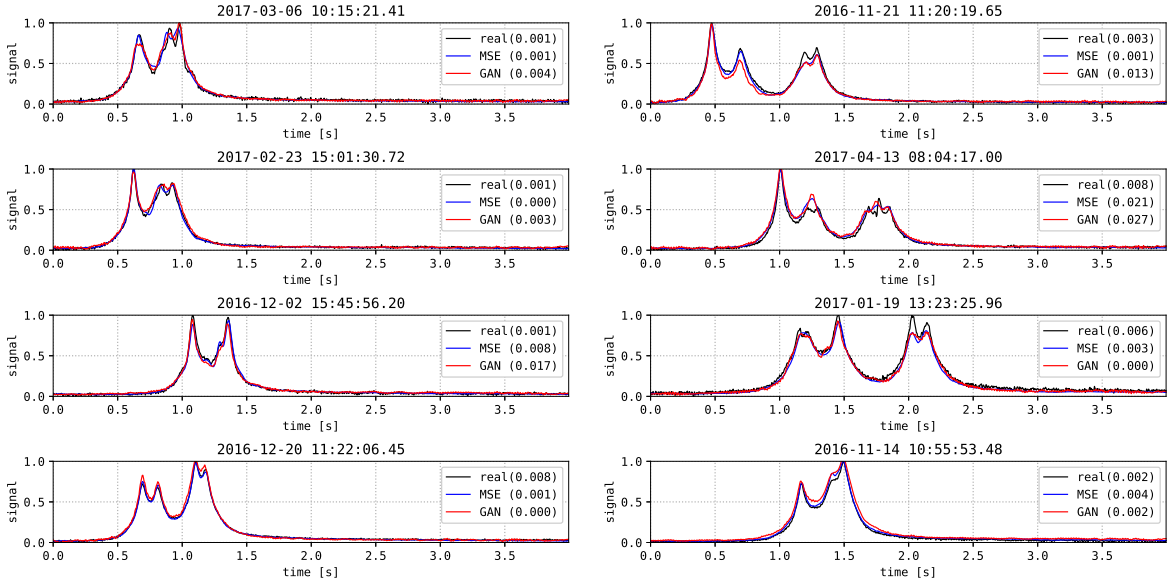


(a) 1st quartile. (b) 3rd quartile.

Figure 5: Strain signal prediction and anomaly scores for strain sensor S1P4 and LtoR vehicles using strain sensor S4P4.

Fig. 6 shows examples of strain signals for RtoL vehicles crossing over strain sensor S4P4, which were estimated using sensor S1P4. Due to the asymmetric structure of the box girder, the shapes of the observed signals were very different from those in Fig. 5. These differences can be seen best in the skirts of the waves, whose heights relative to the peaks were much greater than those in Fig. 5. Again, our proposal successfully simulated these gentle slopes, which start and end just as the vehicle enters and leaves the target span on the bridge.

## 5 DISCUSSION

In this work, we focused mainly on strain signals, although the bridge components may produce various kinds of mechanical responses when a vehicle crosses the bridge. Strain responses on the deck have a strong spatio-temporal locality, with the strain meters having very little reaction to wheel loads at distant points and recovering to the zero points rapidly after the vehicle departs. In contrast, an accelerometer installed at the center of the bridge span can react to distant vehicles, and vibrations at the natural frequencies are likely to be persistent. These properties make bridge vibration analysis more difficult compared with strain analysis.

Whenever abnormal strain responses are found by comparing the predicted and observed responses, we may locate the area of bridge damage by reference to wheel positions on the bridge, as has been explored in some studies (Chen et al., 2014; Huang et al., 2016). Unfortunately, strain sensors are prone to peeling off the surface of bridge components and thus requiring regular inspection. This is one major motive for using less expensive accelerometers instead of strain meters in civil engineering applications (Sekiya et al., 2018). Therefore, in future work, we should develop a GAN for acceleration-response prediction as an alternative to strain-response prediction. Note that the proposed generator may aid in the inspection process for strain sensors.

## 6 CONCLUSION

We have proposed a novel media-fusion approach to long-term bridge health monitoring. The proposed GAN enables direct translation between strain sensors deployed underneath the bridge deck by consulting a surveillance camera on the bridge. The video features may specify vehicle properties including speed, locus, shape, and wheel positions as explanatory variables in the strain prediction. Even though the video may lack information about axle loads, this can be compensated for by analyzing the source sensor signals. We tested our generative network on real observation data, with the results demonstrating highly accurate predictions of measured waveforms.

We expect that bridge damage (and sensor faults) may be revealed by comparing the error distributions of predictions collected soon after the construction of

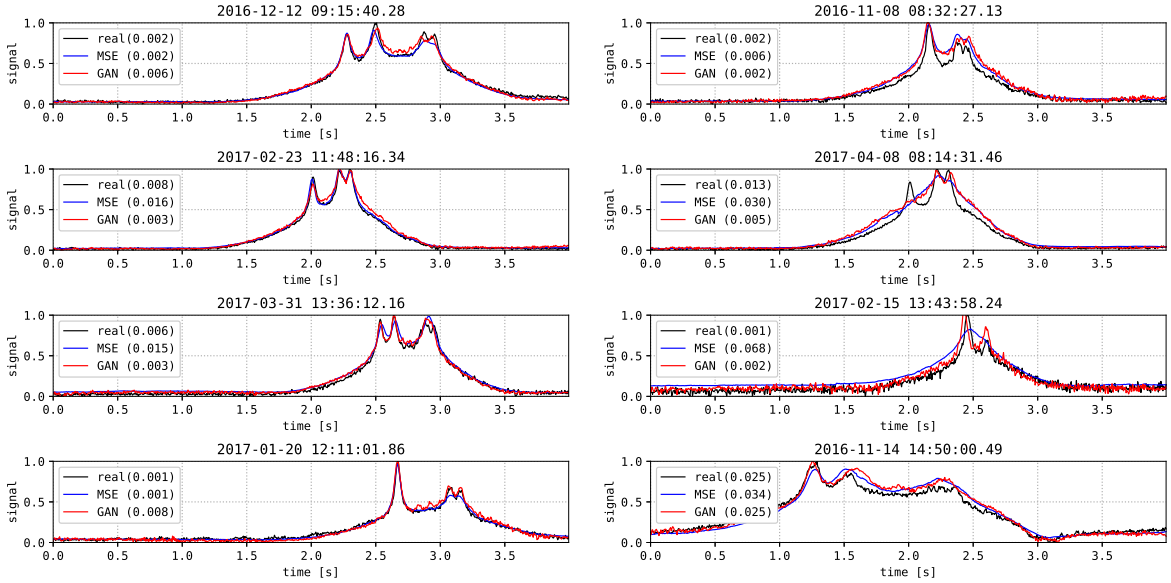


(a) 1st quartile. (b) 3rd quartile.

Figure 6: Strain signal prediction and anomaly scores for strain sensor S4P4 and RtoL vehicles using strain sensor S1P4.

the bridge with the current ones. Compared with the direct comparison of video and strain-signal data in a common feature space, the proposed network enables the visualization of changes in physical quantities for individual bridge components. In future experimental work, we will investigate the connections between the anomaly scores and strain-signal prediction errors. In addition, we also aim to investigate sensor types other than strain meters for use as alternative signal sources.

## ACKNOWLEDGEMENT

This work was supported by the cross-ministerial Strategic Innovation Promotion (SIP) program[3] of the Cabinet Office, Government of Japan.

## REFERENCES

Bicanic, N. and Chen, H.-P. (1997). Damage identification in framed structures using natural frequencies. *IJNME*, 40(23).

Bing, Z., Tiesheng, W., and Shanshan, L. (2011). The research of monitoring model for bridge running. In *ICSSEM*.

Cao, M. S., Sha, G. G., Gao, Y. F., and Ostachowicz, W. (2017). Structural damage identification using damping: a compendium of uses and features. *SMS*, 26(4).

Chen, Z., Cai, Q., Lei, Y., and Zhu, S. (2014). Damage detection of long-span bridges using stress influence lines incorporated control charts. *SCTS*, 57(9).

Dai, W., Dai, C., Qu, S., Li, J., and Das, S. (2017). Very deep convolutional neural networks for raw waveforms. In *ICASSP*.

Donahue, C., McAuley, J., and Puckette, M. (2018). Adversarial audio synthesis. In *ICLR*.

Goodfellow, I. J., Pouget-Abadie, J., Mirza, M., Xu, B., Warde-Farley, D., Ozair, S., Courville, A., and Bengio, Y. (2014). Generative adversarial nets. In *NIPS*.

He, K., Zhang, X., Ren, S., and Sun, J. (2016). Identity mapping in deep residual networks. In *ECCV*.

Huang, Y., Zhu, C., Ye, Y., and Xiao, Y. (2016). Damage detection of arch structure by using deflection influence line. In *SEEIE*.

Isola, P., Zhu, J.-Y., Zhou, T., and Efros, A. A. (2017). Image-to-image translation with conditional adversarial networks. In *CVPR*.

Kawakatsu, T., Kinoshita, A., Aihara, K., Takasu, A., and Adachi, J. (2018a). Adversarial spiral learning approach to strain analysis for bridge damage detection. In *DaWaK*.

Kawakatsu, T., Kinoshita, A., Aihara, K., Takasu, A., and Adachi, J. (2018b). Deep sensing approach to single-sensor bridge weighing in motion. In *EWSHM*.

Kawakatsu, T., Kinoshita, A., Aihara, K., Takasu, A., and Adachi, J. (2019). Deep sensing approach to single-sensor vehicle weighing system on bridges. *IEEE Sensors*, 19(1):243–256.

Kendall, M. G. (1938). A new measure of rank correlation. *Biometrika*, 30(1-2).

Liu, Y. and Wang, X. (2010). The application of BP neural network in cable-stayed bridge construction monitoring. In *ICCIS*.

[3]http://www.jst.go.jp/sip/k07.html

Lydon, M., Taylor, S., Robinson, D., Mufti, A., and OBrien, E. (2015). Recent developmenets in bridge weigh in motion (bwim). *CSHM*, 6.

Ma, Y. and Bi, H. (2011). Cable tension monitoring of suspender arch bridges during cable tension adjustment stage basis on neural network algorithm. In *RSETE*.

Maas, A. L. (2013). Rectifier nonlinearities improve neural network acoustic models. In *ICML*.

Mohamed, B. and Tahar, E. (2017). Remote sensing of damage bridge structure of free vibration by using finite element method based on subspace fitting. In *ICIS*.

Mohamed, B., Tahar, E., and Houria, R. (2017). Remote sensing of damage bridge structure of free vibration by using finite element method based on jerk-energy. In *SERA*.

Neves, A. C., Gonzalez, I., Leander, J., and Karoumi, R. (2017). Structural health monitoring of bridges: a model-free ANN-based approach to damage detection. *CSHM*, 7(5).

Neves, A. C., Gonzalez, I., Leander, J., and Karoumi, R. (2018). A new approach to damage detection in bridges using machine learning. In *EVACES*.

Palanisamy, R. P. and Sim, S.-H. (2015). Bridge scour monitoring using extended kalman filter. In *AESE*.

Quansheng, S., Haiying, Y., Xiaoguang, G., Jiawei, W., and Tong, W. (2010). Application of kalman's filtering method in construction control for cable replacement of the cable-stayed bridge. In *ICECE*.

Radford, A., Metz, L., and Chintala, S. (2016). Unsupervised representation learning with deep convolutional generative adversarial networks. In *ICLR*.

Reddi, S., Kale, S., and Kumar, S. (2018). On the convergence of adam and beyond. In *ICLR*.

Ren, S., He, K., Girshick, R. B., and Sun, J. (2015). Faster R-CNN: Towards real-time object detection with region proposal networks. In *NIPS*.

Sekiya, H., Kubota, K., and Miki, C. (2018). Simplified portable bridge weigh-in-motion system using accelerometers. *JBE*, 23(1).

Shah, A. A., Chowdhry, B. S., Daudpoto, J., and Ali, I. (2018). Transient structural health monitoring of the test bridges using finite element method. In *IMTIC*.

Wu, B., Lu, H., Chen, B., and Gao, Z. (2017). Study on finite element model updating in highway bridge static loading test using spatially-distributed optical fiber sensors. *Sensors*, 17(7).

Xiao, C. and Fang, Z. (2016). Research on multi-sensor information fusion algorithm with sensor fault diagnosis. In *ICIICII*.

Yang, S., Xie, L., Chen, X., Lou, X., Zhu, X., Huang, D., and Li, H. (2017). Statistical parametric speech synthesis using generative adversarial networks under a multi-task learning framework. In *ASRU*.

Yao, Y., Rosasco, L., and Caponnetto, A. (2007). On early stopping in gradient descent learning. *Constructive Approximation*, 26(2).

Yu, Y., Cai, C., and Deng, L. (2016). State-of-the-art review on bridge weigh-in-motion technology. *Advances in Structural Engineering*, 19(9).

Zaurin, R. and Catbas, F. N. (2011). Structural health monitoring using video stream, influence lines, and statistical analysis. *SHM*, 10(3).

Zhang, L., Sun, Z., Zhang, C., Dong, F., and Wei, P. (2018). Numerical investigation of the dynamic responses of long-span bridges with consideration of the random traffic flow based on the intelligent ACC-BPNN model. *IEEE Access*, 6:28520–28529.